

Theoretical investigation of quantum confinement on the Rashba effect in ZnO semiconductor nanocrystals

Cite as: J. Chem. Phys. **152**, 014308 (2020); <https://doi.org/10.1063/1.5128355>

Submitted: 18 September 2019 . Accepted: 12 December 2019 . Published Online: 06 January 2020

 Joseph M. Kasper,  Daniel R. Gamelin, and  Xiaosong Li

COLLECTIONS

Paper published as part of the special topic on [Colloidal Quantum Dots](#)



View Online



Export Citation



CrossMark

ARTICLES YOU MAY BE INTERESTED IN

[Toward the evaluation of intersystem crossing rates with variational relativistic methods](#)

The Journal of Chemical Physics **151**, 084107 (2019); <https://doi.org/10.1063/1.5113815>

[Resolving the ultrafast intersystem crossing in a bimetallic platinum complex](#)

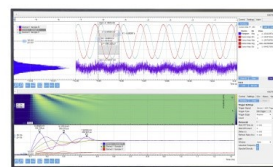
The Journal of Chemical Physics **151**, 114303 (2019); <https://doi.org/10.1063/1.5115169>

[Modeling L_{2,3}-edge X-ray absorption spectroscopy with linear response exact two-component relativistic time-dependent density functional theory](#)

The Journal of Chemical Physics **150**, 234103 (2019); <https://doi.org/10.1063/1.5091807>

Challenge us.

What are your needs for
periodic signal detection?



Zurich
Instruments



Theoretical investigation of quantum confinement on the Rashba effect in ZnO semiconductor nanocrystals

Cite as: J. Chem. Phys. 152, 014308 (2020); doi: 10.1063/1.5128355

Submitted: 18 September 2019 • Accepted: 12 December 2019 •

Published Online: 6 January 2020



View Online



Export Citation



CrossMark

Joseph M. Kasper,  Daniel R. Gamelin,  and Xiaosong Li^{a)} 

AFFILIATIONS

Department of Chemistry, University of Washington, Seattle, Washington 98195, USA

Note: This paper is part of the JCP Special Topic on Colloidal Quantum Dots.

^{a)}Electronic mail: xqli@uw.edu

ABSTRACT

Semiconducting nanocrystals have been the subject of intense research due to the ability to modulate the electronic and magnetic properties by controlling the size of the crystal, introducing dopants, and surface modification. While relatively simple models such as a particle in a sphere can work well to describe moderately sized quantum dots, this approximation becomes less accurate for very small nanocrystals that are strongly confined. In this work, we report all-electron, relativistic *ab initio* electronic structure calculations for a series of ZnO quantum dots in order to study the modulation of the Rashba effect. The impact and magnitude of spin-orbit coupling and crystalline anisotropy on the fine structure of the band-edge excitonic manifold are discussed.

Published under license by AIP Publishing. <https://doi.org/10.1063/1.5128355>

I. INTRODUCTION

The fine control of electronic and magnetic phenomena in nanomaterials is integral to new technologies in computing and data storage. Small colloidal nanocrystals, or quantum dots, have shown great promise in this regard, by allowing properties to be easily tuned through size, dopants, and surface ligands.^{1,2} One of the most important adjustable properties of nanocrystals is the band structure, including the relative ordering of bright and dark excitonic states.³ The precise arrangement of states and their thermal population determines properties such as photoluminescence lifetimes.

Studying quantum dots from the viewpoint of molecular electronic structure theory is extremely powerful to understand the role of localized defects and size-dependent quantum confinement effects.^{4–7} The electronic structure of several types of nanocrystals has been shown to mimic that of a large atom,⁶ so it can be reasonably well-described and understood as a simple particle in a sphere model.⁸ In this case, the excitonic structure is determined by a combination of spin-orbit and symmetry effects that split “P”- and “D”-like superorbitals. In fact, the superatom concept has

previously been applied to study nanoclusters of gold thiolate^{9–11} and show that in these systems, spin-orbit coupling was essential to their theoretical treatment and understanding of visible absorption spectra.¹¹

Much work has been done to understand the role of spin-orbit coupling in bulklike structures using $\mathbf{k} \cdot \mathbf{p}$ band theory and perturbative spin-orbit corrections.^{12–14} For example, in a recent study by Sercel and Efros,¹⁴ a general model for exciton fine structure of II-VI and III-V spherical semiconductor nanocrystals was presented. While these models provide a useful starting point to study band features of moderately sized nanocrystals, they are less amenable to smaller nanocrystals and the impact of localized structural features such as dopants. To our knowledge, there has been no study into how the spin-orbit interaction is manifested in small quantum dots using relativistic *ab initio* molecular electronic structure methods.

Additionally, we note that for studies that have been carried out using band theory, the spin-orbit interaction is usually incorporated perturbatively by a model Hamiltonian (e.g., Pauli) rather than variationally from first principles. In this work, we calculate the electronic structure of semiconducting quantum dots using

two-component Kohn-Sham density functional theory (DFT) that variationally incorporates relativistic effects and spin-orbit coupling. Using excited state calculations, the fine structure of the exciton manifold and the impact of Rashba spin-orbit coupling under strong quantum confinement are uncovered.

II. RELATIVISTIC TREATMENT OF THE RASHBA EFFECT

For crystals without inversion symmetry, it is well-known that the electronic structure is modified by spin-orbit coupling to split low energy excitons as shown in Fig. 1 for a wurtzite lattice that has hexagonal C_{3v} symmetry. The lowest energy exciton manifold is known in the literature as the $1S_{3/2}1S_e$ state. This results from treating the electron and hole particles using the particle in a sphere model and dressing the solutions with appropriate angular momentum functions. That is, the $1S_{3/2}$ valence band hole level corresponds to the product of a 1S Bessel function with the $J = 3/2$ Bloch functions and the $1S_e$ conduction band electron level corresponds to the product of a 1S Bessel function with the $J = 1/2$ Bloch functions.

The breaking of degeneracy of low energy excitons is described within $\mathbf{k} \cdot \mathbf{p}$ theory as a momentum-dependent perturbation. Rashba spin-orbit coupling in the bulk is given by¹⁵

$$\hat{H}_R = (\alpha_R/\hbar)(\mathbf{z} \times \mathbf{p}) \cdot \boldsymbol{\sigma}, \quad (1)$$

where α_R is the Rashba coefficient and \mathbf{z} is the direction of crystal anisotropy. From a molecular orbital point of view, the Rashba effect arises from *both* spin-orbit coupling and crystal field or symmetry lowering effects. In principle, these could be viewed as two successive perturbations as is given schematically in Fig. 1. However, since spin-orbit coupling is known to be quenched by reduced symmetry,¹⁶ one of the two effects may dominate depending on their relative strengths, being either closer to the right or left of the diagram in Fig. 1. Quantum confinement affects both \mathbf{z} and \mathbf{p} in Eq. (1) depending on the nanocrystal size \mathbf{R} . In large nanocrystals that can be well-described by the particle in a sphere model^{8,17,18} because $E \sim \langle p^2 \rangle \sim R^{-2}$ so that \mathbf{p} scales as \mathbf{R}^{-1} and $\mathbf{z} \propto \mathbf{R}$, the overall effect of spin-orbit coupling is independent of the nanocrystal size. For much smaller nanocrystals, however, as the particle in a sphere model breaks down with increasing Coulomb and exchange interaction, there can be larger values of \mathbf{p} for a given confinement \mathbf{R} . As a result, the overall strength of the Rashba spin-orbit coupling can thus be expected to increase for small nanocrystals that are heavily quantum confined, compared with larger nanocrystals

or those in the bulk. In particular, the exchange interaction has been implicated in providing enhancement of spin-orbit coupling in quantum confined systems.¹⁹ Theoretical work on quantum wires has suggested that there exists an optimal value of the potential barrier to the confinement well where the spin-orbit coupling will be maximized.²⁰

While the Schrödinger equation is commonly employed to solve the electronic structure of molecular systems, the natural starting point for including a full description of spin, including spin-orbit coupling and other relativistic effects, is to start with the Dirac equation for an electron. Within the kinetic-balance condition, the Dirac Hamiltonian can be written as^{21,22}

$$\mathbf{H} = \begin{pmatrix} V & \hat{T} \\ \hat{T} & \frac{\mathbf{p}V\mathbf{p}-\hat{T}}{4m^2c^2} \end{pmatrix} + \begin{pmatrix} \mathbf{0}_2 & \mathbf{0}_2 \\ \mathbf{0}_2 & \frac{i\boldsymbol{\sigma}\cdot\mathbf{p}V\times\mathbf{p}}{4m^2c^2} \end{pmatrix}, \quad (2)$$

where V is the scalar potential, c is the speed of light, and m is the electron mass. Spin and orbital angular momenta are coupled through the $\boldsymbol{\sigma} \cdot \mathbf{p}V \times \mathbf{p}$ term: the vector $\boldsymbol{\sigma}$ contains the Pauli spin matrices, and \mathbf{p} is the linear momentum operator. Variational solutions to this Hamiltonian will no longer have a well-defined spin multiplicity, and the eigenstates will have four components. The first term in Eq. (2) is the spin-free portion of the Dirac Hamiltonian, which contains all scalar relativistic effects, while the second term gives rise to spin-couplings. To isolate the effect of spin-orbit coupling, we can compare the results using the full Dirac Hamiltonian with those using only the spin-free part.

Relativistic electronic structure methods based on the Dirac equation employ a four-component wavefunction ansatz.^{21,22} For most chemically relevant studies, approximate two-component methods are usually of sufficient accuracy. In this work, we utilize the exact two-component (X2C) method²³⁻³⁵ that decouples the four-component Hamiltonian and yield a reduced-dimension electronic two-component Hamiltonian. It is of particular note that, unlike effective spin-orbit operators such as Breit-Pauli, the X2C transformed Hamiltonian is bounded from below and does not suffer from variational collapse.^{21,22} Consequently, this two-component method allows for the variational inclusion of relativistic effects at each stage of the calculation.

In this work, we use a direct atomic-orbital based X2C transformation with the torque-free density functional theory (DFT) approach.^{32,35-39} Although X2C can be made formally exact to the 4-component solution, in practice, the two-electron operator is not transformed as this is very computationally expensive.

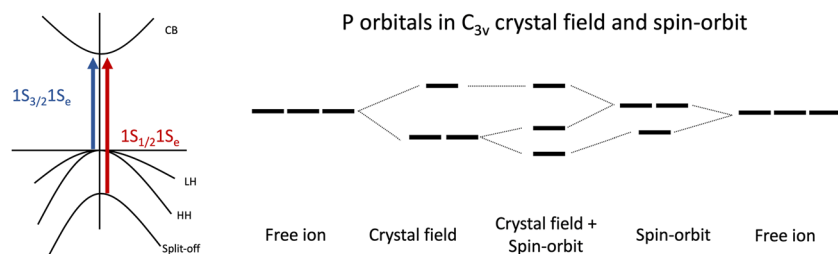


FIG. 1. Schematic diagrams of the valence band structure (left) and valence orbitals (right) for systems with both symmetry-lowering and spin-orbit coupling. Excitations from these orbitals or bands to the lowest unoccupied levels give rise to the lowest energy excitons, known as $1S_{3/2}1S_e$ and $1S_{1/2}1S_e$.

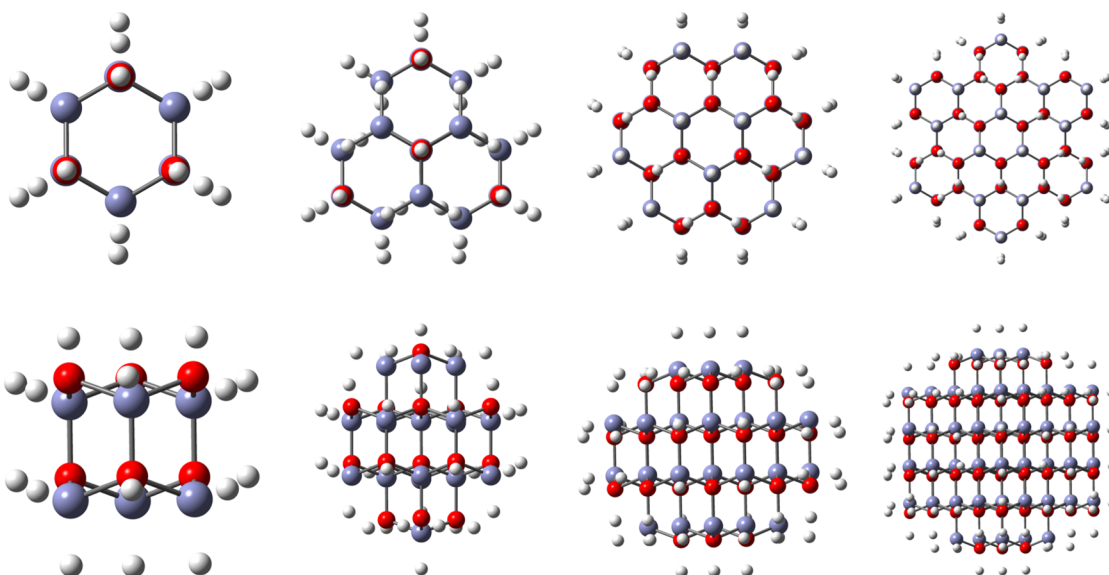


FIG. 2. The ZnO cluster models used: $(\text{ZnO})_6$, $(\text{ZnO})_{17}$, $(\text{ZnO})_{33}$, and $(\text{ZnO})_{84}$.

Instead, in this work, we use an empirical correction to the one-electron spin-orbit terms to account for the neglected two-electron contribution.⁴⁰

III. COMPUTATIONAL DETAILS

Cluster models of ZnO quantum dots ranging in size from a diameter of 0.62–1.87 nm were prepared in accordance with previous studies^{5,6,41–45} and are shown in Fig. 2. A pseudohydrogen capping scheme is used to passivate the dangling bonds on the surface.⁴¹ The clusters use the experimental lattice parameters of $a = 3.249 \text{ \AA}$ and $c = 5.204 \text{ \AA}$ for ZnO. All are approximately spherical but formally have reduced symmetry in the C_{3v} point group. All-electron calculations were performed in a locally modified version of the development version of the Gaussian suite of programs⁴⁶ using the X2C method as described previously and PBE0 exchange-correlation functional.⁴⁷ The 6-31G(d) basis set^{48,49} was used for all atoms.

To quantify the degree of anisotropy in these model quantum dot systems, the ratio between the length of the nanocrystal along the C_3 axis and perpendicular to it are given in Table I. In all nanocrystals except those of size $(\text{ZnO})_{17}$, the hexagonal C_3 axis is shorter than that perpendicular to it. For the nanocrystals of size $(\text{ZnO})_{17}$, the C_3 axis is longer.

TABLE I. The anisotropy ratio between the length of nanocrystals along the C_3 axis and the (x, y) axes.

Size	6	17	33	84
ZnO	0.845	1.301	0.913	0.916

IV. RESULTS AND DISCUSSION

A. Rashba effects on frontier orbitals

The computed densities of states using molecular orbitals are plotted in Fig. 3 and show the smoothing out of discrete states of orbitals into bands as the nanocrystal size is increased. The bandgap decreases with increasing nanocrystal size, as expected. The molecular orbitals at the band edges are shown in Fig. 4. In the absence of spin-orbit coupling (Rashba effect), both the HOMO and HOMO–1 spinor orbitals degenerate with an E symmetry in the C_{3v} point group, while the HOMO–2 having the A_1 symmetry. The orbitals at the conduction band edge appear to be

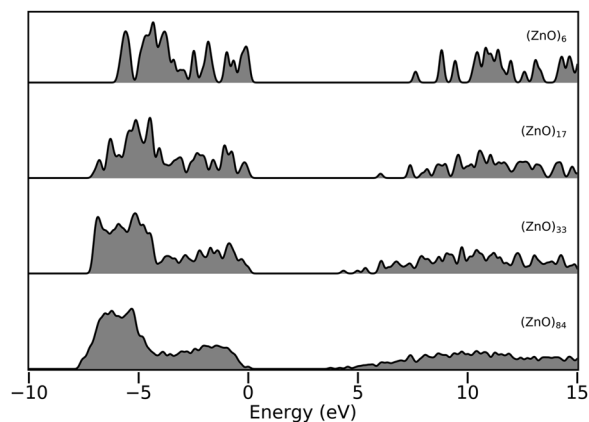


FIG. 3. Computed total densities of states for ZnO quantum dots of increasing size, shifted so that the HOMO lies at 0 eV.

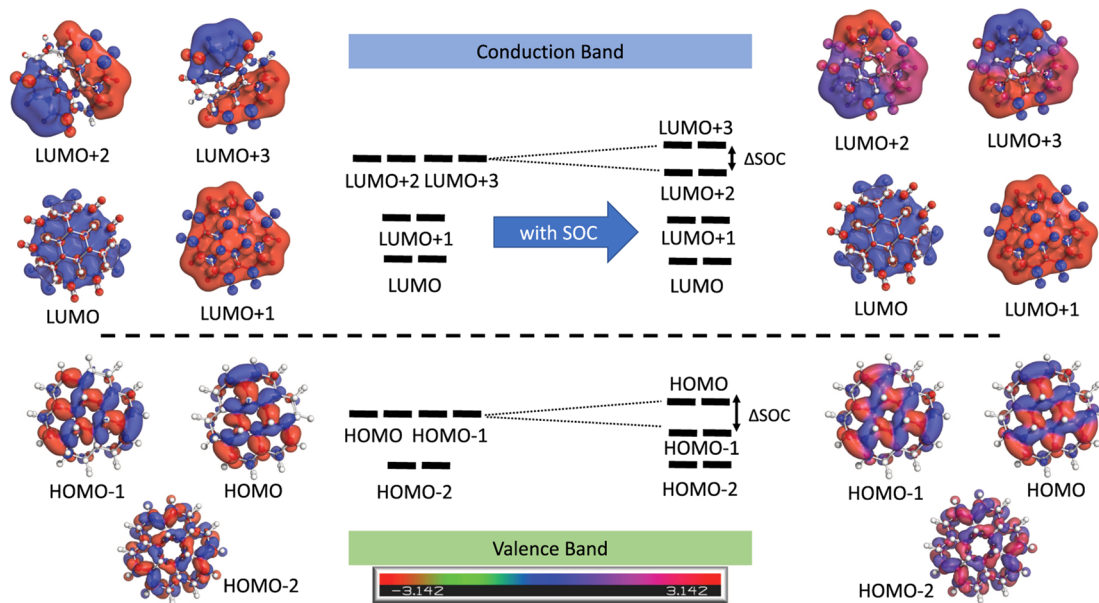


FIG. 4. The molecular orbital diagram of the valence and conduction band edge levels. Due to Kramer's degeneracy, all levels doubly degenerate so only one of the pair of orbitals is shown. MOs from the $(\text{ZnO})_{33}$ are plotted at an isovalue of 0.007 for the magnitude and mapped with the angle between α and β spin-components as shown in the color bar. Values of 0 and π are pure α , while values of $\pm\pi/2$ are pure β .

large atomiclike super-orbitals arising from the spherical potential model.⁶ The LUMO at the conduction band edge is S -type, and LUMO+1 to LUMO+3 are P -type orbitals. If the QDs were perfectly centrosymmetric, we would observe three-fold degenerate P -type orbitals. However, these QDs have a noncentrosymmetric C_{3v} symmetry. As a result, we see a low-symmetry splitting of the P -band into two sublevels, where the higher energy feature consists of two degenerate (P_x, P_y) orbitals and the lower feature corresponds to P_z orbital.

With the inclusion of spin-orbit coupling, we see that the symmetry is further reduced because of mixing between frontier spinor orbitals, which now include both α and β spin-components

as s is no longer a good quantum number. HOMO and HOMO-1 spinors now belong to the $1S_{3/2}$ manifold with $J = 3/2$, whereas HOMO-2 spinors are in the $1S_{1/2}$ level with $J = 1/2$. These variational relativistic calculations show that the inclusion of spin-orbit coupling along with the crystal field and quantum dot anisotropy splits the degenerate E orbitals into two subgroups of $1S_{3/2}$ with different magnetic projections, $M_J = \pm 3/2$ and $M_J = \pm 1/2$, respectively. These correspond to the "heavy" and "light" hole levels in band theory due to their different effective masses.

A quantitative energy level diagram for the ZnO nanocrystals is given in Fig. 5. Of particular note is the different orderings

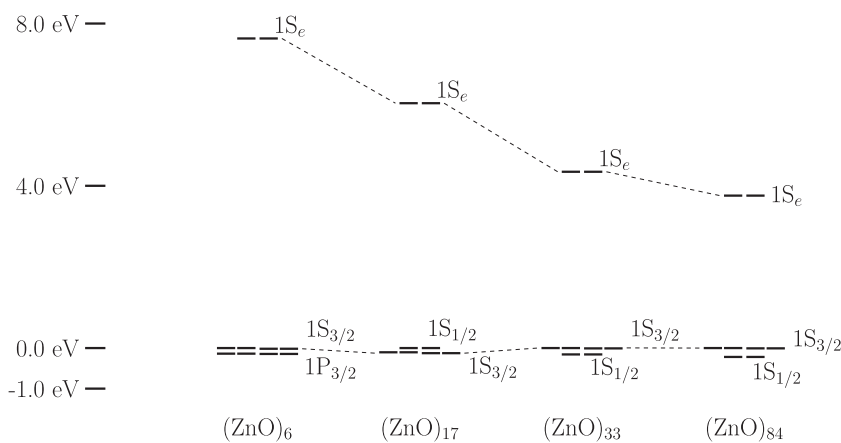


FIG. 5. Energy level diagram for the main states involved in the band-edge excitons of ZnO nanocrystals. Dashed lines connect the $1S_{3/2}$ levels in the valence band as well as the $1S_e$ levels in the conduction band. In the smallest cluster, the $1S_{1/2}$ manifold is deeper in the valence band edge so the level below $1S_{3/2}$ is $1P_{3/2}$.

TABLE II. The magnitude of Rashba-induced splitting in valence band states in ZnO quantum dots, both within the $1S_{3/2}$ manifold and between the $1S_{3/2}$ and $1S_{1/2}$ manifolds (in units of eV).

Size	Within $1S_{3/2}$	Between $1S_{3/2}$ and $1S_{1/2}$
6	0.017	0.134
17	0.022	0.115
33	0.008	0.153
84	0.007	0.266

between levels comprising the $J = 3/2$ and $J = 1/2$ manifolds. It is well-known that the energetic ordering of different J manifolds is very sensitive to the shape of the confining potential.⁵⁰ For the ZnO quantum dots, spin-orbit coupling is relatively small, so crystal field effects and crystal anisotropy play an outsized role compared to other types of II-VI nanocrystals where spin-orbit effects would be larger. In the bulklike systems, the highest lying valence band levels are the $1S_{3/2}$ and $1S_{1/2}$ manifolds. This is the structure seen in the larger $(\text{ZnO})_{33}$ and $(\text{ZnO})_{84}$ nanocrystals, in which $1S_{3/2}$ is above $1S_{1/2}$. For the smaller dots, deviations from this usual pattern are observed. In the $(\text{ZnO})_{17}$ cluster, a reversed level structure is seen in which the $1S_{1/2}$ level actually moves above the $1S_{3/2}$ level because the crystal field acts with the opposite sign due to the C_3 axis being elongated rather than shortened. For the smallest cluster, $(\text{ZnO})_6$, the $1S_{1/2}$ manifold is further inside from the valence band edge so that the $1P_{3/2}$ level is immediately below the $1S_{3/2}$ level. Since the splitting between the distinct angular momentum manifolds in the valence band is most important to understanding the band-edge excitonic features, we focus on the magnitude of the splitting in the valence band and tabulate these values in Table II. The splitting within the $1S_{3/2}$ manifold is the difference between “light” and “heavy” holes. Although there is no clear trend in the data, the ZnO results suggest the magnitude of shape anisotropy and the strength of the crystal field strongly influence the Rashba effect within the $S_{3/2}$ manifold.

B. Rashba effects on effective mass

$\mathbf{k} \cdot \mathbf{p}$ theory and the effective mass model have been useful for describing the energetics and spin-orbit coupling of nanocrystals that are more bulklike.^{13,51} The effective masses of the electrons and holes can be calculated from the *ab initio* band structure by fitting them to an appropriate model. In the case of nanocrystals that are confined in all directions, the particle in a sphere model has been used.^{6,8} In this model, the energy levels depend on quantum numbers n and l and are given by

$$E_{n,l} = \frac{\beta_{n,l}^2 \hbar^2}{2m_e^* R^2}, \quad (3)$$

where R is the radius of the nanocrystal, m_e^* is the effective mass, and $\beta_{n,l}$ is the n th zero of the l th spherical Bessel function. The first four levels, $1S$, $1P$, $1D$, and $2S$, were used to fit the effective masses for both the valence band maximum and conduction band minimum.

TABLE III. The calculated effective masses of electrons and holes, Bohr radii, and binding energies E_b for ZnO quantum dots.

Molecule	Without spin-orbit				With spin-orbit			
	m_h^*	m_e^*	Bohr radius	E_b (eV)	m_h^*	m_e^*	Bohr radius	E_b (eV)
$(\text{ZnO})_6$	5.972	3.814	3.65	0.877	5.932	3.814	3.66	0.874
$(\text{ZnO})_{18}$	4.597	1.878	6.37	0.502	4.589	1.877	6.38	0.501
$(\text{ZnO})_{33}$	3.396	1.286	9.11	0.351	3.372	1.285	9.13	0.350
$(\text{ZnO})_{84}$	1.631	0.813	15.66	0.204	1.621	0.813	15.70	0.204

The effective masses are also related to the size of the exciton. Assuming a dielectric constant $\epsilon = 8.5$ for ZnO,⁵² the Bohr radius r_B for the exciton can be estimated as⁵³

$$r_B = \epsilon \left(\frac{1}{m_h^*} + \frac{1}{m_e^*} \right). \quad (4)$$

Additionally, the exciton binding energies E_b can be estimated from the model and are given by⁵⁴

$$E_b = \frac{e^2}{\epsilon r_B} = \frac{m^*}{e^2}, \quad (5)$$

where e is the electron charge (1 in atomic units) and m^* is the effective reduced mass.

The estimated values for the ZnO nanocrystals are given in Table III. As a broad trend, the effective mass of both the hole and electron sharply decrease with increasing nanocrystal size. The spin-orbit interaction has a larger effect on the valence band than conduction band, consistent with previous studies that show the effective field due to spin-orbit coupling is different for electrons and holes.¹² These data also suggest that the spin-orbit interaction lowers the average effective mass for the hole states. As expected from the decreased effective mass of the holes, the spin-orbit interaction slightly increases the size of exciton. This also leads to a slight decrease in the exciton binding energy.

C. Optical transitions and exciton splitting

Quantum confinement and the Rashba effect are also manifested in the linear absorption spectrum. While the quantum confinement effect is known to blue-shift the first bright excitation with decreasing nanocrystal size, it also affects spin-orbit coupling and causes a mixing of the excitonic levels.^{50,55} The Rashba effect and crystalline anisotropy split the first exciton, denoted as $1S_{3/2}1S_e$, into sublevels that are sensitive to the quantum confinement. Spin-orbit coupling associated with the $1S_{3/2} \rightarrow 1S_e$ excitation gives rise to two manifolds of the $1S_{3/2}1S_e$ excitons, $J = 2, 1$ with 5- and 3-fold degeneracy, respectively. Crystalline anisotropy further splits states that have different magnetic quantum numbers, e.g., $M_J = \pm 2, \pm 1, 0$ for the $J = 2$ manifold and $M_J = \pm 1, 0$ for the $J = 1$ manifold. States that are split from the $J = 2$ (or $J = 1$) manifold are denoted as “L” (or “U”) for “Lower” (or “Upper”) energy groups.

The computed exciton fine structure for the $(\text{ZnO})_{33}$ quantum dot is assigned as given in Table IV. According to the

TABLE IV. The exciton fine structure for $(\text{ZnO})_{33}$ quantum dots.

Sublevel	Excitation energy (eV)	Oscillator Strength
0^L	3.677	0.0000
0^U	3.677	0.0001
$\pm 1^L$	3.681	0.0003
$\pm 2^L$	3.686	0.0000
$\pm 1^U$	3.738	0.0384

selection rule in $\mathbf{k}\cdot\mathbf{p}$ theory for bulk materials,¹⁴ only the $\pm 1^U$, $\pm 1^L$, and 0^U sublevels are optically allowed transitions, and $\pm 2^L$ and 0^L sublevels are forbidden. The computed results for quantum dots suggest that optical transition selection rules for the period bulk system are also maintained in finite, quantum confined structures. The strongest allowed excitonic transition is to the $\pm 1^U$ states that are above 6 lower-lying forbidden or weakly allowed transitions.

The ordering of $1S_{3/2}1S_e$ sublevels strongly depends on the relative strength of crystalline anisotropy and the Rashba effect. In quantum confined systems, strong crystalline anisotropy can lead to large splittings. Of particular note for the $(\text{ZnO})_{33}$ quantum dot, the 0^U level is split enough from the “Upper” group that it overlaps with the states from the lower manifold.

For the smaller $(\text{ZnO})_{17}$ nanocrystal (Table V), the higher degree of anisotropy leads to a much stronger crystal field relative to the strength of spin-orbit coupling. As a result, the 0^U level actually drops below the 0^L sublevel so that the lowest energy exciton is now optically active. In the smallest $(\text{ZnO})_6$ crystal, the magnitude of crystal field anisotropy is lower again so that the 0^L dark exciton is the lowest energy, as given in Table VI.

These results are shown graphically in Fig. 6. The oscillator strength is almost completely localized in the $\pm 1^U$ transitions, with

TABLE V. The exciton fine structure for $(\text{ZnO})_{17}$ quantum dots.

Sublevel	Excitation energy (eV)	Oscillator Strength
0^U	4.938	0.0007
0^L	4.941	0.0000
$\pm 1^L$	4.951	0.0003
$\pm 2^L$	4.962	0.0000
$\pm 1^U$	5.191	0.1484

TABLE VI. The exciton fine structure for $(\text{ZnO})_6$ quantum dots.

Sublevel	Excitation energy (eV)	Oscillator Strength
0^L	6.116	0.0000
0^U	6.117	0.0001
$\pm 1^L$	6.124	0.0001
$\pm 2^L$	6.133	0.0000
$\pm 1^U$	6.464	0.1057

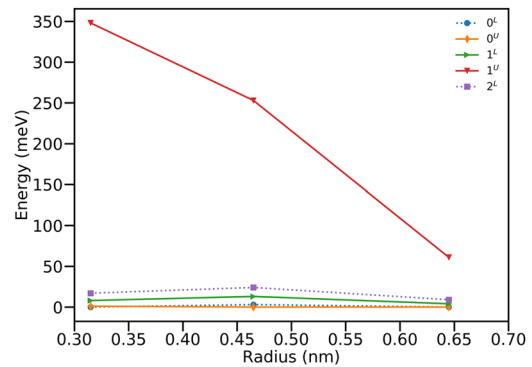


FIG. 6. The exciton fine structure levels for ZnO quantum dots. The lowest energy state is set to zero.

lowered transition strength in the other optically active modes. This agrees with other work in the literature, which shows the oscillator strength of the $\pm 1^L$ transitions decaying to zero for small nanocrystal radius and being redistributed into the $\pm 1^U$ manifold.⁵⁶

In Table VII, the splittings within and between the different angular momentum manifolds are given. While the splitting between sublevels with different M_J projections in the lower manifold Δ_L has a strong dependence on the crystal field, the splitting

TABLE VII. Computed fine structure splittings in ZnO quantum dots (in eV). Δ_L is the splitting in the lower manifold, Δ_U is the splitting in the upper manifold, and Δ_{U-L} is the splitting between the mean energy of the two manifolds.

Nanocrystal	Δ_L	Δ_U	Δ_{U-L}
$(\text{ZnO})_6$	0.008	0.347	0.1662
$(\text{ZnO})_{17}$	0.010	0.253	0.1132
$(\text{ZnO})_{33}$	0.005	0.061	0.0262

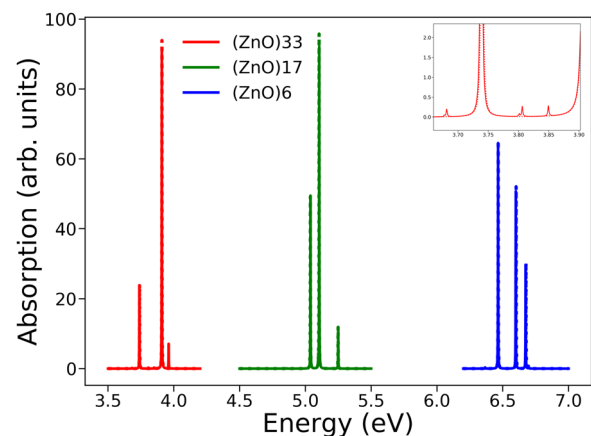


FIG. 7. The optical absorption spectra of ZnO quantum dots calculated by TDDFT. The dashed lines indicate spin-orbit free calculations, while the solid traces include spin-orbit coupling. The inset shows a zoom-in on the $(\text{ZnO})_{33}$ features, where dark states gain intensity under spin-orbit coupling by singlet-triplet mixing.

TABLE VIII. MO transition amplitudes for the first bright excited state in $(\text{ZnO})_{17}$.

MOs	Amplitude (%)
HOMO-17 \rightarrow LUMO+1	1.99
HOMO-16 \rightarrow LUMO	1.99
HOMO-1 \rightarrow LUMO	18.82
HOMO-1 \rightarrow LUMO+1	25.92
HOMO \rightarrow LUMO	25.92
HOMO \rightarrow LUMO+1	18.92
NTO 1	$\lambda = 0.481$
NTO 2	$\lambda = 0.481$

in the upper manifold Δ_U and between the mean energies of the two manifolds Δ_{U-L} has a strong dependence on the nanocrystal size. One reason for this difference in exciton manifolds is that the heavy holes with $M_J = \pm 3/2$ feel both “short”- and “long”-range exchange, while the light holes with $M_J = \pm 1/2$ only feel “short”-range exchange.¹⁴ This difference is enhanced as the nanocrystals are more confined.

In Fig. 7, the computed absorption spectra are plotted, both with and without the inclusion of spin-orbit coupling. All peaks are broadened with a Lorentzian lineshape with a FWHM of 0.005 eV. Analysis of the transition amplitudes shows that the band-edge excitons are indeed well-described by a hole in the $1S_{3/2}$ manifold and an electron in the $1S_e$ level, although this analysis also shows some mixing with deeper valence band states than those depicted in the diagram given in Fig. 4. In the case of the $(\text{ZnO})_{17}$ cluster, the transition amplitudes and resulting natural transition orbitals (NTO) eigenvalues given in Table VIII show about 4% contribution from lower lying bands; however, the simple picture of a single particle excitation from the $1S_{3/2}$ levels in the valence band is still largely true, with nearly 96% recovered in the dominant NTOs. The NTOs for the

first bright excited state are plotted in Fig. 8. Transition from O $2p$ orbitals goes into an s -like superorbital delocalized over the entire cluster, consistent with the previous model.

V. CONCLUSIONS

In this work, we have performed *ab initio* electronic structure calculations that incorporate relativistic effects to demonstrate the effect of quantum confinement on spin-orbit coupling that affects the band-edge excitonic manifold in ZnO quantum dots. This allows for the study of the Rashba effect in small, highly quantum-confined systems where the band model used in $\mathbf{k} \cdot \mathbf{p}$ theory can break down. In particular, we have found that the “Upper” and “Lower” exciton manifolds can mix and overlap in small ZnO nanocrystals, where already small spin-orbit coupling is further reduced by symmetry-lowering crystal field effects. The cluster models used here can easily be adapted to explore the role of surface and ligand modifications, dopants, and other defects on the ground state electronic structure and fine structure of the excitonic manifold.

Although there are no k -vectors defined in 0D materials, the phenomena observed in this work share an important similarity with the Rashba effect—the combination of spin-orbit with other reduced symmetry and shape effects. In particular, the reduced symmetry environment here is due to changes to the confining potential in the dimension of one axis (the z axis), as is the case in larger 2D materials. In 0D materials, since the translational symmetry is absent, the time-reversal symmetry is maintained. As a result, there is no Zeeman splitting. In principle, both Rashba and Dresselhaus effects are present in the calculation because we employed a variational spin-orbit approach where all orders of perturbation are included. However, it is very difficult to differentiate these effects because of the lack of k -vectors in the analysis.

ACKNOWLEDGMENTS

This research is supported by the University of Washington Molecular Engineering Materials Center, funded by the National Science Foundation (Grant No. DMR-1719797). The development of the relativistic electronic structure method is supported by the U.S. Department of Energy (Grant No. DE-SC0006863). This work was facilitated through the use of advanced computational, storage, and networking infrastructure provided by the Hyak supercomputer system and funded by the STF at the University of Washington and the National Science Foundation (Grant No. MRI-1624430).

REFERENCES

- ¹R. Beaulac, S. T. Ochsnein, and D. R. Gamelin, in *Semiconductor Quantum Dots*, 2nd ed., edited by V. I. Klimov (CRC Press, Boca Raton, 2010), p. 397.
- ²G. Armelles, A. Cebollada, A. García-Martín, and M. U. González, “Magneto-plasmonics: Combining magnetic and plasmonic functionalities,” *Adv. Opt. Mater.* **1**, 10–35 (2013).
- ³M. A. Becker, R. Vaxenburg, G. Nedelcu, P. C. Sercel, A. Shabaev, M. J. Mehl, J. G. Michopoulos, S. G. Lambrakos, N. Bernstein, J. L. Lyons, T. Stöferle, R. F. Marht, M. V. Kovalenko, D. J. Norris, G. Rainó, and A. L. Efros, “Bright triplet excitons in caesium lead halide perovskites,” *Nature* **553**, 189 (2018).
- ⁴L.-W. Wang and J. Li, “First-principles thousand-atom quantum dot calculations,” *Phys. Rev. B* **69**, 153302 (2004).

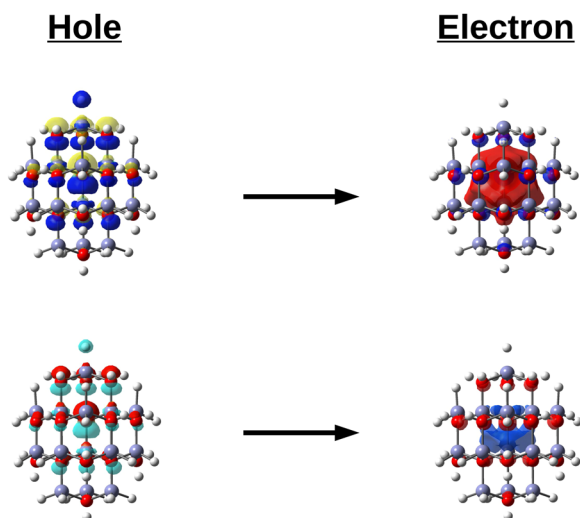


FIG. 8. The NTOs of the first bright excited state in $(\text{ZnO})_{17}$. There are two sets of orbitals (top and bottom), corresponding to the α and β spins.

- ⁵E. Badaeva, J. W. May, J. Ma, D. R. Gamelin, and X. Li, "Characterization of excited-state magnetic exchange in Mn²⁺-doped ZnO quantum dots using time-dependent density functional theory," *J. Phys. Chem. C* **115**, 20986–20991 (2011).
- ⁶J. J. Goings, A. M. Schimpf, J. W. May, R. W. Johns, D. R. Gamelin, and X. Li, "Theoretical characterization of conduction-band electrons in photodoped and aluminum-doped zinc oxide (AZO) quantum dots," *J. Phys. Chem. C* **118**, 26584–26590 (2014).
- ⁷H. D. Nelson, X. Li, and D. R. Gamelin, "Computational studies of the electronic structures of copper-doped CdSe nanocrystals: Oxidation states, Jahn–Teller distortions, vibronic bandshapes, and singlet–triplet splittings," *J. Phys. Chem. C* **120**, 5714–5723 (2016).
- ⁸H. Liu, C. K. Brozek, S. Sun, D. B. Lingerfelt, D. R. Gamelin, and X. Li, "A hybrid quantum-classical model of electrostatics in multiply charged quantum dots," *J. Phys. Chem. C* **121**, 26086–26095 (2017).
- ⁹M. Walter, J. Akola, O. Lopez-Acevedo, P. D. Jadzinsky, G. Calero, C. J. Ackerson, R. L. Whetten, H. Grönbeck, and H. Häkkinen, "A unified view of ligand-protected gold clusters as superatom complexes," *Proc. Natl. Acad. Sci. U. S. A.* **105**, 9157–9162 (2008).
- ¹⁰J. Akola, M. Walter, R. L. Whetten, H. Häkkinen, and H. Grönbeck, "On the structure of thiolate-protected Au₂₅," *J. Am. Chem. Soc.* **130**, 3756–3757 (2008).
- ¹¹D.-e. Jiang, M. Kühn, Q. Tang, and F. Weigend, "Superatomic orbitals under spin-orbit coupling," *J. Phys. Chem. Lett.* **5**, 3286–3289 (2014).
- ¹²K. Nash, P. Calcott, L. Canham, and R. Needs, "Spin-orbit interaction, triplet lifetime, and fine-structure splitting of excitons in highly porous silicon," *Phys. Rev. B* **51**, 17698 (1995).
- ¹³J. Fu and M. Wu, "Spin-orbit coupling in bulk ZnO and GaN," *J. Appl. Phys.* **104**, 093712 (2008).
- ¹⁴P. C. Sercel and A. L. Efros, "Band-edge exciton in CdSe and other II–VI and III–V compound semiconductor nanocrystals-revisited," *Nano Lett.* **18**, 4061–4068 (2018).
- ¹⁵A. Manchon, H. C. Koo, J. Nitta, S. Frolov, and R. Duine, "New perspectives for Rashba spin-orbit coupling," *Nat. Mater.* **14**, 871 (2015).
- ¹⁶F. S. Ham, "Effect of linear Jahn-Teller coupling on paramagnetic resonance in a ²E state," *Phys. Rev.* **166**, 307 (1968).
- ¹⁷L. A. Brus, "Simple model for the ionization potential, electron affinity, and aqueous redox potentials of small semiconductor crystallites," *J. Chem. Phys.* **79**, 5566–5571 (1983).
- ¹⁸L. E. Brus, "Electron electron and electron-hole interactions in small semiconductor crystallites: The size dependence of the lowest excited electronic states," *J. Chem. Phys.* **80**, 4403–4409 (1984).
- ¹⁹G.-H. Chen and M. Raikh, "Exchange-induced enhancement of spin-orbit coupling in two-dimensional electronic systems," *Phys. Rev. B* **60**, 4826 (1999).
- ²⁰R. Li, Z.-H. Liu, Y. Wu, and C. Liu, "The impacts of the quantum-dot confining potential on the spin-orbit effect," *Sci. Rep.* **8**, 7400 (2018).
- ²¹K. G. Dyall and K. Fægri, Jr., *Introduction to Relativistic Quantum Chemistry* (Oxford University Press, 2007).
- ²²M. Reiher and A. Wolf, *Relativistic Quantum Chemistry*, 2nd ed. (Wiley-VCH, 2015).
- ²³W. Kutznigg and W. Liu, "Quasirelativistic theory equivalent to fully relativistic theory," *J. Chem. Phys.* **123**, 241102 (2005).
- ²⁴W. Liu and D. Peng, "Infinite-order quasirelativistic density functional method based on the exact matrix quasirelativistic theory," *J. Chem. Phys.* **125**, 044102 (2006).
- ²⁵D. Peng, W. Liu, Y. Xiao, and L. Cheng, "Making four- and two-component relativistic density functional methods fully equivalent based on the idea of from atoms to molecule," *J. Chem. Phys.* **127**, 104106 (2007).
- ²⁶M. Ilias and T. Saue, "An infinite-order relativistic Hamiltonian by a simple one-step transformation," *J. Chem. Phys.* **126**, 064102 (2007).
- ²⁷W. Liu and D. Peng, "Exact two-component Hamiltonians revisited," *J. Chem. Phys.* **131**, 031104 (2009).
- ²⁸W. Liu, "Ideas of relativistic quantum chemistry," *Mol. Phys.* **108**, 1679–1706 (2010).
- ²⁹T. Saue, "Relativistic Hamiltonians for chemistry: A primer," *ChemPhysChem* **12**, 3077–3094 (2011).
- ³⁰Z. Li, Y. Xiao, and W. Liu, "On the spin separation of algebraic two-component relativistic Hamiltonians," *J. Chem. Phys.* **137**, 154114 (2012).
- ³¹D. Peng, N. Middendorff, F. Weigend, and M. Reiher, "An efficient implementation of two-component relativistic exact-decoupling methods for large molecules," *J. Chem. Phys.* **138**, 184105 (2013).
- ³²F. Egidi, J. J. Goings, M. J. Frisch, and X. Li, "Direct atomic-orbital-based relativistic two-component linear response method for calculating excited-state fine structures," *J. Chem. Theory Comput.* **12**, 3711–3718 (2016).
- ³³J. J. Goings, J. M. Kasper, F. Egidi, S. Sun, and X. Li, "Real time propagation of the exact two component time-dependent density functional theory," *J. Chem. Phys.* **145**, 104107 (2016).
- ³⁴L. Konecny, M. Kadek, S. Komorovsky, O. L. Malkina, K. Ruud, and M. Repisky, "Acceleration of relativistic electron dynamics by means of X2C transformation: Application to the calculation of nonlinear optical properties," *J. Chem. Theory Comput.* **12**, 5823–5833 (2016).
- ³⁵F. Egidi, S. Sun, J. J. Goings, G. Scalmani, M. J. Frisch, and X. Li, "Two-component non-collinear time-dependent spin density functional theory for excited state calculations," *J. Chem. Theory Comput.* **13**, 2591–2603 (2017).
- ³⁶J. E. Peralta, G. E. Scuseria, and M. J. Frisch, "Noncollinear magnetism in density functional calculations," *Phys. Rev. B* **75**, 125119 (2007).
- ³⁷G. Scalmani and M. J. Frisch, "A new approach to noncollinear spin density functional theory beyond the local density approximation," *J. Chem. Theory Comput.* **8**, 2193–2196 (2012).
- ³⁸I. W. Bulik, G. Scalmani, M. J. Frisch, and G. E. Scuseria, "Noncollinear density functional theory having proper invariance and local torque properties," *Phys. Rev. B* **87**, 035117 (2013).
- ³⁹A. Petrone, D. B. Williams-Young, S. Sun, T. F. Stetina, and X. Li, "An efficient implementation of two-component relativistic density functional theory with torque-free auxiliary variables," *Eur. Phys. J. B* **91**, 169 (2018).
- ⁴⁰J. C. Boettger, "Approximate two-electron spin-orbit coupling term for density-functional-theory DFT calculations using the Douglas-Kroll-Hess transformation," *Phys. Rev. B* **62**, 7809–7815 (2000).
- ⁴¹E. Badaeva, Y. Feng, D. R. Gamelin, and X. Li, "Investigation of pure and Co²⁺-doped ZnO quantum dot electronic structures using the density functional theory: Choosing the right functional," *New J. Phys.* **10**, 055013 (2008).
- ⁴²E. Badaeva, C. M. Isborn, Y. Feng, S. T. Ochsenein, D. R. Gamelin, and X. Li, "Theoretical characterization of electronic transitions in Co²⁺- and Mn²⁺-doped ZnO nanocrystals," *J. Phys. Chem. C* **113**, 8710–8717 (2009).
- ⁴³Y. Feng, E. Badaeva, D. R. Gamelin, and X. Li, "Excited-state double exchange in manganese-doped ZnO quantum dots: A time-dependent density-functional study," *J. Phys. Chem. Lett.* **1**, 1927–1931 (2010).
- ⁴⁴J. W. May, J. Ma, E. Badaeva, and X. Li, "Effect of excited-state structural relaxation on midgap excitations in Co²⁺-doped ZnO quantum dots," *J. Phys. Chem. C* **118**, 13152–13156 (2014).
- ⁴⁵S. A. Fischer, D. B. Lingerfelt, J. W. May, and X. Li, "Non-adiabatic molecular dynamics investigation of photoionization state formation and lifetime in Mn²⁺-doped ZnO quantum dots," *Phys. Chem. Chem. Phys.* **16**, 17507–17514 (2014).
- ⁴⁶M. J. Frisch, G. W. Trucks, H. B. Schlegel, G. E. Scuseria, M. A. Robb, J. R. Cheeseman, G. Scalmani, V. Barone, G. A. Petersson, H. Nakatsuji, X. Li, M. Caricato, A. V. Marenich, J. Bloino, B. G. Janesko, R. Gomperts, B. Mennucci, H. P. Hratchian, J. V. Ortiz, A. F. Izmaylov, J. L. Sonnenberg, D. Williams-Young, F. Ding, F. Lipparini, F. Egidi, J. Goings, B. Peng, A. Petrone, T. Henderson, D. Ranasinghe, V. G. Zakrzewski, J. Gao, N. Rega, G. Zheng, W. Liang, M. Hada, M. Ehara, K. Toyota, R. Fukuda, J. Hasegawa, M. Ishida, T. Nakajima, Y. Honda, O. Kitao, H. Nakai, T. Vreven, K. Throssell, J. A. Montgomery, Jr., J. E. Peralta, F. Ogliaro, M. J. Bearpark, J. J. Heyd, E. N. Brothers, K. N. Kudin, V. N. Staroverov, T. A. Keith, R. Kobayashi, J. Normand, K. Raghavachari, A. P. Rendell, J. C. Burant, S. S. Iyengar, J. Tomasi, M. Cossi, J. M. Millam, M. Klene, C. Adamo, R. Cammi, J. W. Ochterski, R. L. Martin, K. Morokuma, O. Farkas, J. B. Foresman, and D. J. Fox, Gaussian Development Version Revision I.11+, Gaussian, Inc., Wallingford, CT, 2016.

- ⁴⁷J. P. Perdew, K. Burke, and M. Ernzerhof, "Generalized gradient approximation made simple," *Phys. Rev. Lett.* **77**, 3865–3868 (1996).
- ⁴⁸R. Krishnan, J. S. Binkley, R. Seeger, and J. A. Pople, "Self-consistent molecular orbital methods. XX. A basis set for correlated wave functions," *J. Chem. Phys.* **72**, 650–654 (1980).
- ⁴⁹T. Clark, J. Chandrasekhar, G. W. Spitznagel, and P. V. R. Schleyer, "Efficient diffuse function-augmented basis sets for anion calculations. III. The 3-21+ G basis set for first-row elements Li–F," *J. Comput. Chem.* **4**, 294–301 (1983).
- ⁵⁰F. Korychenko and J. Kossut, "Diluted magnetic semiconductor quantum dots: An extreme sensitivity of the hole Zeeman splitting on the aspect ratio of the confining potential," *Phys. Rev. B* **70**, 205317 (2004).
- ⁵¹J.-W. Wang and S.-S. Li, "Excitonic bright-to-dark transition induced by spin-orbit coupling," *Appl. Phys. Lett.* **92**, 012106 (2008).
- ⁵²N. Ashkenov, B. Mbenkum, C. Bundesmann, V. Riede, M. Lorenz, D. Spemann, E. Kaidashev, A. Kasic, M. Schubert, M. Grundmann, G. Wagner, H. Neumann, V. Darakchieva, H. Arwin, and B. Monemar, "Infrared dielectric functions and phonon modes of high-quality ZnO films," *J. Appl. Phys.* **93**, 126–133 (2003).
- ⁵³J. I. Pankove, *Optical Processes in Semiconductors* (Dover, 1975).
- ⁵⁴M. Dvorak, S.-H. Wei, and Z. Wu, "Origin of the variation of exciton binding energy in semiconductors," *Phys. Rev. Lett.* **110**, 016402 (2013).
- ⁵⁵L. Lew Yan Voon, R. Melnik, B. Lassen, and M. Willatzen, "Influence of aspect ratio on the lowest states of quantum rods," *Nano Lett.* **4**, 289–292 (2004).
- ⁵⁶M. Kuno, J.-K. Lee, B. O. Dabbousi, F. V. Mikulec, and M. G. Bawendi, "The band edge luminescence of surface modified CdSe nanocrystallites: Probing the luminescing state," *J. Chem. Phys.* **106**, 9869–9882 (1997).